
Frustratingly Easy Uncertainty Estimation for Distribution Shift

Tiago Salvador
Mila, McGill University

Vikram Voleti
Mila, Université de Montréal

Alexander Iannantuono
UBC Okanagan

Adam Oberman
Mila, McGill University

Abstract

Distribution shift is an important concern in deep image classification, produced either by corruption of the source images, or a complete change, with the solution involving domain adaptation. While the primary goal is to improve accuracy under distribution shift, an important secondary goal is uncertainty estimation: evaluating the probability that the prediction of a model is correct. While improving accuracy is hard, uncertainty estimation turns out to be frustratingly easy. Prior works have appended uncertainty estimation into the model and training paradigm in various ways. Instead, we show that we can estimate uncertainty by simply exposing the original model to corrupted images, and performing simple statistical calibration on the image outputs. Our frustratingly easy methods demonstrate superior performance on a wide range of distribution shifts as well as on unsupervised domain adaptation tasks, measured through extensive experimentation.

1 Introduction

As deep learning models become more ubiquitous, it has become increasingly critical to estimate their predictive uncertainty i.e. how reliable their predictions are. This is particularly important in healthcare, financial, and legal settings where a human user makes a decision aided by a deep learning model. The predictive uncertainty of a deep classification model is typically provided by an estimate of the class-wise probabilities of a given sample.

The baseline predictive uncertainty method is to simply use the softmax probabilities of the model as a surrogate for the class-wise probabilities [Hendrycks and Gimpel, 2017] (we will refer to this as the **Vanilla** method). However, such probability estimates are known to lead to overconfident models [Nguyen et al., 2015], and several approaches have been proposed to calibrate these probabilities. These methods include non-Bayesian ones such as **Temperature Scaling** (TS) [Guo et al., 2017], dropout [Srivastava et al., 2014, Gal and Ghahramani, 2016], and model ensembles [Lakshminarayanan et al., 2017], as well as Bayesian approaches such as Stochastic Variational Bayesian Inference (SVBI) for deep learning [Graves, 2011, Blundell et al., 2015, Louizos and Welling, 2016, 2017, Wen et al., 2018], among others.

All these approaches produce calibrated probabilities for in-distribution data with varying degrees of success. However, it has been found that the quality of the uncertainty predictions deteriorates significantly for data under *distributional shift* [Hendrycks and Dietterich, 2019, Ovadia et al., 2019].

Ovadia et al. [2019] demonstrate this by performing a large-scale benchmark analysis of existing methods for predictive uncertainty under dataset shift. In particular, CIFAR-10 and ImageNet trained models were evaluated on (i) synthetic shifts using their corrupted counterparts CIFAR-10-C and ImageNet-C [Hendrycks and Dietterich, 2019]. Other types of dataset shifts include (ii) natural shifts,

Table 1: Comparison of different calibration methods.

Calibration Methods	works with domain shift	no features	no retuning	no target images
Vanilla	✗	✓	✓	✓
TS	✗	✓	✓	✓
CPCS	✓	✗	✗	✗
TransCal	✓	✗	✗	✗
SAC (Ours)	✓	✓	✓	✗
STS (Ours)	✓	✓	✓	✓

such as from ImageNet to ImageNet-v2 [Recht et al., 2019] or ImageNet-Sketch [Wang et al., 2019], and (iii) domain shift, from synthetic images to real images, such as in Office-Home [Venkateswara et al., 2017], or VisDA-2017 [Peng et al., 2017].

In this work, we propose two frustratingly easy and effective post hoc methods for model calibration under distributional shift : Surrogate Adaptive Calibration (SAC), and Surrogate Temperature Scaling (STS). Our focus is on calibration for unsupervised distribution shift, where only unlabeled images of the test distribution are available. Our methods provide superior results among comparable methods, on the three types of distribution shift mentioned above: (i) synthetic shifts (CIFAR-10-C, ImageNet-C), (ii) natural shifts (ImageNet-V2, ImageNet-Sketch), and (iii) domain shifts (Office-Home, VisDA-2017). The key idea is that we can estimate distribution shift using just the model outputs, by comparing with known (arbitrary) corruption of in-distribution data.

Our methods can be combined with training-based calibration methods, and show impressive results on never seen types of corruptions. Our methods require no intermediate features from the model, and do not need any retraining, retuning, or additional training of models.

2 Related Work

Models trained on a given dataset are unlikely to perform as well on a shifted data [Hendrycks and Dietterich, 2019, Ovadia et al., 2019], and there are inevitable tradeoffs between accuracy and robustness [Chun et al., 2020]. Several approaches have been proposed to increase model robustness, typically evaluated on the benchmark corrupted datasets CIFAR-10-C and ImageNet-C. Methods such as Hendrycks et al. [2019a] show that fine-tuning a pre-trained model can improve the quality of the uncertainty estimates compared to training a model from scratch, but it does not improve accuracy. In contrast, we propose simple calibration methods that require no additional training or fine-tuning.

Simply training models against corruptions can fail to make models robust to new corruptions [Vasiljevic et al., 2016, Geirhos et al., 2018]. However, Hendrycks et al. [2020] train models with a carefully designed new data augmentation technique called AUGMIX, and are able to improve both robustness and uncertainty measures. In contrast, our work applies a data augmentation technique at the calibration stage, which avoids having to retrain the models from scratch, and can be a simple post-hoc fix to calibrate trained models.

Nado et al. [2020] argue that the internal activations of deep models also suffer from distributional shift in the presence of shifted data. They thus propose to recompute the batch normalization coefficients at prediction time using a sample of the unlabeled images from the test distribution. While the accuracy, and ultimately the calibration, was improved for synthetic shifts (ImageNet-C), it degraded the accuracy for natural shifts (ImageNet-v2). Moreover, their work requires knowing the internal activations of the model, and hence is a white-box calibration which works only on deep neural networks. In contrast, we improve any model’s calibration treating it as a black box, and hence do not require to know its internal functionalities.

Krishnan and Tickoo [2020] introduced a new loss function, and demonstrated that it can be used as post-hoc calibration method leading to improved accuracy and uncertainty measures against new corruptions. This work can be seen as orthogonal to ours as the methods we propose here can be used as an add-on to any post-hoc supervised calibration method.

Shao et al. [2020] propose a confidence calibration method that uses an auxiliary classifier to identify mis-classified samples, thus allowing them to be assigned low confidence. However, it requires a small sample of labeled test data. In contrast, our method does not require target labels.

While the above works focus on synthetic shifts modeled by noise corruptions, natural shifts (e.g. clipart to real images) are of greater interest. These are prominent in unsupervised domain adaptation, where only unlabeled examples from the test distribution are available. Many algorithms have been proposed to leverage these during training, which can be split into two main groups: (a) *moment matching*, which look to minimize the Maximum Mean Discrepancy [Gretton et al., 2012] between source (labeled) and target (unlabeled) images at the feature level (e.g. DAN [Long et al., 2015], JAN [Long et al., 2017]); and (b) *adversarial training*, inspired by the success of Generative Adversarial Networks (GANs) [Goodfellow et al., 2014]: DANN [Ganin et al., 2016] introduced a domain discriminator that differentiates source features from target features, competing with the feature extractor; CDAN [Long et al., 2018] improved upon DANN by conditioning the model on the classifier predictions; SAFN [Xu et al., 2019] observe that the accuracy degradation from source to target model arises from the smaller feature of the target domain in comparison to the source domain, and propose an Adaptive Feature Norm approach to fix it; MDD [Zhang et al., 2019] proposed a new domain adaptation margin theory; MCC [Jin et al., 2020] proposed a new loss to minimize class confusion i.e. the tendency of the classifier to confuse correct and ambiguous classes for the target examples. However, these methods only focus on accuracy, and do not leverage calibration for uncertainty estimation.

Domain adaptation algorithms improve accuracy at the expense of model calibration [Wang et al., 2020]. To fix this, Park et al. [2020] proposed **CPCS**, an approach based on importance weighting to correct for covariate shift in data by deriving an upper bound on the expected calibration error. **TransCal** [Wang et al., 2020] extended the Temperature Scaling method into domain adaption, and achieved more accurate calibration with lower bias and variance, without introducing any hyperparameters. (Concurrent work by Gupta et al. [2020] presents some preliminary simulations also using importance weighting, but limited to Random Forest and binary classifiers.)

However, both CPCS and TransCal require access to the model’s features to train an additional domain classifier, which is then used to compute the importance weights. In contrast, our methods only require the softmax probabilities of the model, thereby treating the model as a black-box, and can be extended to classifiers other than neural networks. Moreover, CPCS and TransCal need to be re-tuned for every new corruption to compute new importance weights. In contrast, our calibration methods require no retraining of any sort, and performs calibration for each surrogate set a priori.

3 Calibration

3.1 Supervised Calibration

Consider the K -class classification problem, where $\mathbf{x} \in \mathcal{X}$ is a set of inputs such as images, and $y \in \{1, \dots, K\}$ denotes the corresponding labels. The inputs and labels are drawn i.i.d. from the joint distribution $p(\mathbf{x}, y)$, and y is a sample from the conditional distribution $p(y | \mathbf{x})$.

A classifier $f(\mathbf{x})$ is trained using a training dataset $\mathcal{D}_{\text{in}}^{\text{train}}$, with hyper-parameters selected using a validation/calibration dataset $\mathcal{D}_{\text{in}}^{\text{cal}}$. The datasets $\mathcal{D}_{\text{in}}^{\text{train}}$ and $\mathcal{D}_{\text{in}}^{\text{cal}}$ consist of finite samples drawn i.i.d. from $p(\mathbf{x}, y)$.

Typically when f is a deep neural network, $f : \mathcal{X} \rightarrow [0, 1]^K$ has a terminal softmax layer applied to linear outputs $g(\mathbf{x})$, i.e. $f(\mathbf{x}) = \text{softmax}(g(\mathbf{x}))$. Hence, the model f outputs a probability distribution on the K labels given an input \mathbf{x} from \mathcal{X} (our analysis can be generalized to the case where the model outputs scores). The predicted class \hat{y} is given by the most likely output:

$$\hat{y}(\mathbf{x}) = \arg \max_k f(\mathbf{x})_k; \quad p^{\max}(\mathbf{x}) = \max_k f(\mathbf{x})_k \tag{1}$$

The model confidence (or uncertainty) c_k for label k is defined as the probability that the true label is k given the classifier’s softmax output for that label $f(\mathbf{x})_k$:

$$c(\mathbf{x}; p, f)_k = \mathbb{P}_{p(\tilde{\mathbf{x}}, y)} [y = k | f(\tilde{\mathbf{x}})_k = f(\mathbf{x})_k] \tag{2}$$

We write $c(\mathbf{x}; p, f)$ to emphasize c ’s dependence on both f and $p(\mathbf{x}, y)$, since the distribution will change below. We shorten the notation whenever it is clear from context.

The goal of *supervised calibration* [Park et al., 2020] is to estimate the calibrated probabilities c empirically by \hat{c} using a finite set of labeled samples $\mathcal{D}_{\text{in}}^{\text{cal}}$ drawn from $p(\mathbf{x}, y)$. The error between the true and the estimated confidences is typically measured by Expected Calibration Error (ECE \downarrow) [Guo et al., 2017]:

$$\text{ECE} = \mathbb{E}_{p(\mathbf{x}, y)} [\|c(\mathbf{x}) - \hat{c}(\mathbf{x})\|] \quad (3)$$

Vanilla : $\hat{c}(\mathbf{x}) = f(\mathbf{x})$, i.e. the *Vanilla* approach simply estimates $c(\mathbf{x})$ as the softmax probabilities $f(\mathbf{x})$.

In general, these softmax probabilities are not an accurate prediction of the class probabilities [Domingos and Pazzani, 1996]. In particular, for deep neural network models they are overconfident predictions [Guo et al., 2017]. They become even more overconfident under distribution shift [Ovadia et al., 2019].

Temperature scaling: $\hat{c}(\mathbf{x}) = \text{softmax}(g(\mathbf{x})/T)$, and an optimal T is estimated [Guo et al., 2017] by minimizing the negative log likelihood loss on the calibration set $\mathcal{D}_{\text{in}}^{\text{cal}}$.

3.2 Covariate Calibration for Unsupervised Domain Adaptation

Unsupervised domain adaptation is the case where in addition to labeled images $\mathcal{D}_{\text{in}}^{\text{train}}$ from the source distribution $p(\mathbf{x}, y)$, we also have unlabeled images $\mathcal{D}_{\text{out}}^{\text{test}}$ from a target distribution $q(\mathbf{x}, y)$ that is different from p . Here, q is said to have a covariate shift from p , i.e. $q(y|\mathbf{x}) = p(y|\mathbf{x})$ but $q(\mathbf{x}) \neq p(\mathbf{x})$ [Shimodaira, 2000]. The standard way of training models involves using images only from p . However, domain adaptation methods may leverage the unlabeled images $\mathcal{D}_{\text{out}}^{\text{test}}$ from q during training.

The goal of *covariate calibration* [Park et al., 2020] is to estimate calibrated probabilities c for q :

$$c(\mathbf{x}; q, f)_k = \mathbb{P}_{q(\tilde{\mathbf{x}}, y)} [y = k \mid f(\tilde{\mathbf{x}})_k = f(\mathbf{x})_k] \quad (4)$$

The challenge lies in the fact that while we are given a calibration dataset of labeled examples $\mathcal{D}_{\text{in}}^{\text{cal}}$ drawn from p , we only have a dataset of unlabeled examples $\mathcal{D}_{\text{out}}^{\text{test}}$ drawn from q . In other words, Equation 4 requires labels to estimate c , which are not available.

Temperature Scaling (TS) does not tackle this directly, and assumes that the calibrated probabilities for p must work well on q .

CPCS [Park et al., 2020] and **TransCal** [Wang et al., 2020] compute an importance weight for each sample in $\mathcal{D}_{\text{in}}^{\text{cal}}$ using samples from $\mathcal{D}_{\text{in}}^{\text{train}}$ and $\mathcal{D}_{\text{out}}^{\text{test}}$, and then use a weighted version of temperature scaling:

1. Compute $w(\mathbf{x}) = q(\mathbf{x})/p(\mathbf{x}) \forall \mathbf{x} \in \mathcal{D}_{\text{in}}^{\text{cal}}$, using $\mathcal{D}_{\text{out}}^{\text{test}}$
2. Optimize T in temperature scaling by minimizing a weighted calibration error.

CPCS [Park et al., 2020] minimizes the Brier Score [DeGroot and Fienberg, 1983] weighted by w . **TransCal** [Wang et al., 2020] minimizes ECE weighted by w , with additional terms to correct for bias and variance in the expectations.

CPCS and TransCal need to compute importance weights to estimate the distribution shift, and then calibrate through temperature scaling. This unfortunately implies that new weights and temperatures need to be computed for every new type of corruption, and every new intensity.

4 Our methods

We conjecture that *distribution shift can be imitated by model output shift* for calibration. While the former is a complex distribution shift, the latter is one dimensional and can be handled by simple statistical techniques. Our solution is to find a surrogate shifted dataset (where the labels are known), with a p^{max} model distribution similar to the unknown one. Then, we can use this surrogate dataset to calibrate the unknown one in a supervised fashion by simply setting $c(\mathbf{x}; q, f)_k = c(\mathbf{x}; q^*, f)$, where q^* denotes the surrogate dataset distribution.

We empirically observe that these values indeed match, provided the $p^{\text{max}}(\tilde{\mathbf{x}})$ distribution for $\tilde{\mathbf{x}} \sim q^*$ is close to the $p^{\text{max}}(\mathbf{x})$ distribution for $\mathbf{x} \sim q$. Figure 1 TOP shows the p^{max} distributions of corrupted

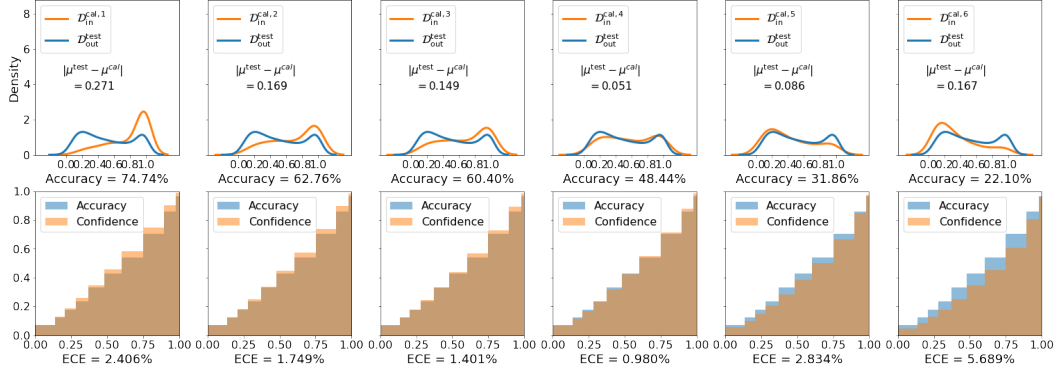


Figure 1: TOP: Probability density (using kernel density estimation) of $\mathcal{D}_{\text{out}}^{\text{test}}$ (blue) obtained by corrupting ImageNet test images with the “elastic transform” at intensity 2, and the p^{max} distribution of each calibration set $\mathcal{D}_{\text{in}}^{\text{cal},j}$ (orange) obtained by corrupting ImageNet-cal images with varying intensity of a different corruption “pixelate”. BOTTOM: The respective accuracy and calibration confidence. The minimum calibration error is achieved precisely when the means of the distributions are the closest.

ImageNet-test set, and six surrogate calibration sets synthesized from the ImageNet-calibration set by adding increasing levels of a different corruption. It can be seen that the 4th surrogate distribution represents the closest match with the test distribution. Indeed, in Figure 1 BOTTOM, we see that this corresponds to the least calibration error.

Our approach is motivated by the theory on domain adaptation by Ben-David et al. [2007, 2010] which suggests that successful transfer across distributions is one where the model cannot identify to which distribution the input observation belongs to. We achieve precisely this by matching with a surrogate distribution.

Choice of supervised calibration method: We first choose a supervised calibration method, and adapt it for covariate calibration. We chose Temperature Scaling [Guo et al., 2017], and show that this simple calibration method is sufficient to estimate uncertainty reliably. Note that any other calibration method could be used instead of Temperature Scaling as part of our methods.

While more sophisticated supervised calibration methods have recently been proposed [Kull et al., 2019, Rahimi et al., 2020], Temperature Scaling remains a competitive baseline. Moreover, CPCS [Park et al., 2020] and TransCal [Wang et al., 2020], which are the most relevant prior methods for covariate calibration, both utilize Temperature Scaling. This makes it ideal for a fair comparison.

4.1 Surrogate Adaptive Calibration (SAC)

Synthesize surrogate calibration sets: Given a set of finite samples $\mathcal{D}_{\text{in}}^{\text{cal}}$ drawn from $p(\mathbf{x}, y)$ not seen during the training of the model, we form J distinct calibration sets $\mathcal{D}_{\text{in}}^{\text{cal},j}$, $j = \{1, \dots, J\}$, by corrupting the data with a known corruption at different levels of intensity. This step is equivalent to drawing samples from distributions $q^j(\mathbf{x}, y)$, $j = \{1, \dots, J\}$ with a covariate shift from $p(\mathbf{x}, y)$. However, unlike the unlabelled data drawn from q , the labels of q^j are known. Therefore, we can apply supervised calibration methods on each q^j to obtain confidence estimates. The final uncertainty estimate is then provided by the best q^j according to some metric. We expand on the number of surrogate calibration sets and choice of corruption in Section 7.3.

Calibrate the surrogate sets: For each calibration set $\mathcal{D}_{\text{in}}^{\text{cal},j}$, we define by T_j the optimal temperature obtained through Temperature Scaling. Thus, recalling that g denotes the model’s scores pre-softmax, we have $\hat{c}(\mathbf{x}; q^j, f) = \text{softmax}(g(\mathbf{x})/T_j)$.

Then, given a test set of samples $\mathcal{D}_{\text{out}}^{\text{test}} = \{\mathbf{x}_1, \dots, \mathbf{x}_m\}$ drawn from $q(\mathbf{x}, y)$,

1. Calculate the mean of the p^{\max} values of the test images:

$$\mu^{\text{test}} = \mu(p^{\max}(\mathcal{D}_{\text{out}}^{\text{test}})) = \frac{1}{|\mathcal{D}_{\text{out}}^{\text{test}}|} \sum_{\mathbf{x} \in \mathcal{D}_{\text{out}}^{\text{test}}} p^{\max}(\mathbf{x}) \quad (5)$$

2. Record the surrogate calibration set with the mean of its p^{\max} values i.e. $\mu^{\text{cal},j} = \mu(p^{\max}(\mathcal{D}_{\text{in}}^{\text{cal},j}))$ closest to μ^{test} :

$$i = \arg \min_j |\mu^{\text{test}} - \mu^{\text{cal},j}| \quad (6)$$

3. Calibrate $\mathcal{D}_{\text{out}}^{\text{test}}$ according to the surrogate calibration set with the closest mean:

$$\hat{c}(\mathbf{x}; q, f) = \hat{c}(\mathbf{x}; q^i, f) \quad (7)$$

Our calibration method is simple, and computationally efficient. The most expensive step is in evaluating the calibration images and respective corruptions with the classifier. This can be done efficiently since the number of images is relatively low. By relying on Temperature Scaling, which requires solving a one parameter optimization, the supervised calibration on each surrogate set can also be computed quickly. These can be computed and stored a priori. Therefore, at the evaluation stage we only need to compare the means.

4.2 Surrogate Temperature Scaling (STS)

We also propose a (frustratingly) easy and effective variant of SAC. Instead of choosing one surrogate calibration set $\mathcal{D}_{\text{in}}^{\text{cal},i}$ with the closest mean p^{\max} to the test set, we calibrate according to the union of all the synthesized surrogate calibration sets $\mathcal{D}_{\text{in}}^{\text{cal},j}$. We find that this performs better than the prior methods, and just as effectively as SAC.

We compare our methods' characteristics with those of relevant prior methods in Table 1.

5 Evaluation Metric

As is typically the case, we evaluate calibration error in terms of the probability of *correct classification* i.e. Top-1 correctness:

$$c^{\text{Top-1}}(\mathbf{x}; q, f) = \mathbb{P}_{q(\tilde{\mathbf{x}}, y)} [y = \hat{y}(\tilde{\mathbf{x}}) \mid p^{\max}(\tilde{\mathbf{x}}) = p^{\max}(\mathbf{x})] \quad (8)$$

Our estimated Top-1 confidence estimate is naturally given by:

$$\hat{c}^{\text{Top-1}}(\mathbf{x}; q, f) = \max_k \hat{c}^{\text{Top-1}}(\mathbf{x}; q, f)_k. \quad (9)$$

We then measure Top-1 ECE, by binning the data based on the probability of the most probable class according to the classifier i.e. $p^{\max}(\mathbf{x})$. For each bin B_m , $m \in \{1, \dots, M\}$, we estimate the true Top-1 model confidence by:

$$c^{\text{Top-1}}(B_m) = \frac{1}{|B_m|} \sum_{(\mathbf{x}, y) \in B_m} \mathbf{1}_{\hat{y}(\mathbf{x})=y} \quad (10)$$

where $\mathbf{1}_{\hat{y}(\mathbf{x})=y}$ is 1 if $\hat{y}(\mathbf{x}) = y$, else 0.

Similarly, the empirical bin model confidence is:

$$\hat{c}^{\text{Top-1}}(B_m) = \frac{1}{|B_m|} \sum_{(\mathbf{x}, y) \in B_m} \hat{c}^{\text{Top-1}}(\mathbf{x}; q, f) \quad (11)$$

Then, the bin ECE is calculated as the binned version of Eq. 3, the weighted-average of the absolute difference between $c^{\text{Top-1}}(B_m)$ and $\hat{c}^{\text{Top-1}}(B_m)$:

$$ECE = \sum_{m=1}^M \frac{|B_m|}{N} |c^{\text{Top-1}}(B_m) - \hat{c}^{\text{Top-1}}(B_m)| \quad (12)$$

where N is the total number of test samples, and $|B_m|$ is the number of samples in bin B_m . The actual value of ECE depends on the binning procedure used: equally spaced, or equally sized. Equal spacing leads to bins with very few samples since deep learning models have high accuracy and therefore, if calibrated, high confidence. To mitigate this issue, we use equal sized bins similar to Nixon et al. [2019] and Hendrycks et al. [2019b]. In our experiments, we use $M = 15$ equal-sized bins.

6 Datasets

6.1 Synthetic shifts

We evaluate on synthetic distribution shift using the CIFAR-10 and ImageNet datasets, and their corrupted counterparts CIFAR-10-C and ImageNet-C [Hendrycks and Dietterich, 2019]. The latter were formed by applying common real-world corruptions (16 in total) at 5 levels of intensity to the 10,000 test images of CIFAR-10, and the 50,000 test images of ImageNet. Corruptions include brightness (variations in daylight intensity), Gaussian noise (in low-lighting conditions) and Defocus blur (when the image is out of focus). See the Appendix for examples of each of the corruptions used. We chose 5,000 images to form our \mathcal{D}_{in}^{cal} . The remaining images form \mathcal{D}_{in}^{test} , and their corrupted versions form \mathcal{D}_{out}^{test} .

6.2 Natural shifts

We evaluate on natural distribution shift using:

1. ImageNet-V2 [Recht et al., 2019] dataset, which was designed to be as similar as possible to the original ImageNet dataset, but the data collection process took place a decade after ImageNet. It contains three different versions resulting from different sampling strategies: Matched-Frequency (MF), Threshold-0.7 (Thr), Top-Images (TI).
2. ImageNet-Sketch [Wang et al., 2019] dataset, which shares the same 1000 classes as ImageNet but all the images are black and white sketches.

6.3 Domain Adaptation

In the context of Domain Adaptation, we consider:

1. Office-Home [Venkateswara et al., 2017], a medium-scale dataset with 65 classes and 4 domains: Artistic (A), Clipart (C), Product (P) and Real-World (R). Models are trained using labeled images of one domain (source) and unlabeled image of a different domain (target). We consider all 12 combinations of domain shifts.
2. VISDA-2017, a large-scale dataset with a 12-class object recognition task and a large domain shift from synthesis-to-real images. The training set contains 152,000 synthetic images generated by rendering 3D models, while the test set has 55,000 real object images sampled from Microsoft COCO [Lin et al., 2014].

We consider two different partitions of each domain depending on if it is used as a source or target distribution. When used as the source distribution, we do a 80/20 split into \mathcal{D}_{in}^{train} and \mathcal{D}_{in}^{cal} . When used as a target distribution, we do a 50/50 split. One split is used during training, and the other forms our \mathcal{D}_{out}^{test} . We present calibration on \mathcal{D}_{out}^{test} .

7 Experimental details

7.1 Relevant comparisons

Our proposed method performs post-training confidence calibration for unsupervised domain adaptation. Thus we compare our SAC and STS methods to CPCS [Park et al., 2020] and TransCal [Wang et al., 2020]. As additional baselines, we also consider Vanilla (softmax probabilities) and Temperature Scaling (TS) [Guo et al., 2017].

7.2 Models

Source-only: For the CIFAR10 models, we used the ResNet-20 pretrained model provided in the Github repo “Sandbox for training deep learning networks”¹ [Sémery, 2021]. During training, the images were randomly distorted using horizontal flips and random crops and their brightness, contrast and saturation were jittered.

¹<https://github.com/osmr/imgclsmob>

For the ImageNet models, we used pretrained ResNet-50 provided by PyTorch, which used the same data augmentation during training. Hence, brightness, contrast and saturation, together with the corruption used in our SAC and STS methods, are removed from CIFAR10-C and ImageNet-C when testing.

Domain Adaptation: We trained models using the Transfer Learning Library Github repo² [Jiang et al., 2020]. The different domain adaptation methods we used include DAN [Long et al., 2015], JAN [Long et al., 2017], CDAN [Long et al., 2018], MDD [Zhang et al., 2019], SAFN [Xu et al., 2019], MCC [Jin et al., 2020].

7.3 Choices in SAC and STS

Our calibration methods SAC and STS require the synthesis of multiple calibration sets of varying corruption intensity from the original calibration set. We used “pixelate” as the corruption, and generated $J = 6$ calibration sets.

Choice of surrogate sets: We form $J = 6$ calibration sets $\mathcal{D}_{in}^{cal,j}$, since CIFAR10-C and ImageNet-C contain 5 levels of corruption intensity. We chose to include the original calibration set, and 5 surrogate sets with increasing corruption intensity. For $j = 1$, we simply take the images in \mathcal{D}_{in}^{cal} . For $j > 1$, we take their “pixelate”-corrupted counterparts with intensity level $j - 1$.

Choice of corruption for calibration: We find that the choice of corruption for calibration does not affect the overall performance significantly. We performed a cross-validation study over the choice of corruption used to generate the calibration sets (always leaving it out of the corruptions used at test time). Figure 5 (in the appendix) plots the mean and variance of the ECE across different choices for calibration corruptions.

It is to be noted that the corrupted images at test time have *never been seen by the model*, either at the training stage or the calibration stage. Despite this, our easy calibration methods perform quite well. The \mathcal{D}_{out}^{test} of the synthetically shifted CIFAR-10-C and Imagenet-C are formed by perturbing the images in the respective \mathcal{D}_{in}^{test} with corruptions different from those used during training and calibration, i.e. not brightness, contrast, saturation, or pixelate. Hence, $\mathcal{D}_{in}^{cal,j}$ and \mathcal{D}_{out}^{test} are completely disjoint. Despite this, our calibration shows improved results on \mathcal{D}_{out}^{test} in the cases of covariate shift.

Alternative distances: In Eq. 6, instead of the distance between the means, any other difference between distributions could be used. We tried the Kolmogorov-Smirnoff statistic, and the Wasserstein distance between the cumulative distributions of the p^{max} values (see Figure 6 in the appendix), and do not find significant change in performance from using the mean.

More efficient mean calculation: Instead of computing the mean of the full \mathcal{D}_{out}^{test} , we computed it for a random subset of only 100 samples, and found similar performance (see Figure 7 in the appendix). As both CPCS and TransCal require substantially higher samples for an effective estimation of the importance weights, this is a significant advantage of our SAC method.

8 Results

8.1 Synthetic shift

We applied the different calibration methods mentioned before to the CIFAR10 and ImageNet trained models, and evaluated their calibration on CIFAR10-C and ImageNet-C. We report the ECE means across the different corruptions in Figure 2. For a more detailed comparison, we have included in the appendix (see Figure 9) a box plot with different quantiles summarizing the ECE results for each method and intensity shift. Importantly, we leave out brightness, contrast and saturation corruption since they were used during training as well as the pixelate corruption used by both STS and SAC method during calibration.

Both figures show that SAC and STS *consistently outperform* all other methods. They minimize ECE the most across all levels of corruption intensity, with even better performance at higher levels of intensity.

²<https://github.com/thuml/Transfer-Learning-Library>

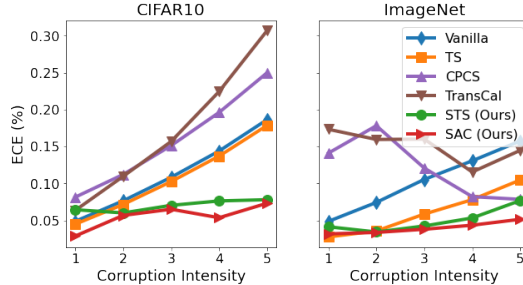


Figure 2: Mean ECE % (lower is better) across corruption types (synthetic distribution shift) for 5 corruption intensities using different calibration methods: Vanilla, Temperature Scaling (TS), CPCS [Park et al., 2020], TransCal [Wang et al., 2020], our Surrogate Temperature Scaling (STS), and our Surrogate-Adaptive Calibration (SAC). Our methods perform the best among all methods across all intensities, with the greatest improvement at higher intensities.

Table 2: ECE % (lower is better) for natural distribution shifts on ImageNet.

	ImageNet-V2			ImageNet-Sketch
	MF	Thr	TI	
Vanilla	8.77	4.88	3.23	22.29
TS	4.81	2.49	1.87	16.09
CPCS	5.29	3.26	5.85	38.79
TransCal	12.26	4.43	1.99	52.24
SAC (Ours)	4.44	2.49	1.86	10.71
STS (Ours)	4.71	2.39	1.90	15.86

CPCS and TransCal are able to improve calibration at higher corruption intensities only for the ImageNet model. Since the models are trained using only the source distribution, there is a large discrepancy between source (clean images) and target (corrupted images) distributions, which leads to bad importance weight estimation, and ultimately poor calibration by CPCS and TransCal.

8.2 Natural shift

The results of evaluating the calibration methods on all three versions of ImageNet-V2 and ImageNet-Sketch are displayed in Table 2. Once again, SAC and STS provide the best results.

8.3 Domain Adaptation

For the Office-Home dataset, we trained a different model for each of the 12 combinations of domain shifts, using the CDAN adaptation algorithm [Long et al., 2018]. We applied the different calibration methods on the split of the target distribution not seen during training, so as to mimic a more challenging case and close to real-world application. The results are displayed in Table 3. Our simple STS method provides the best calibration in 6 out of the 12 domain shifts.

As for the VisDA-2017 dataset, which contains only one domain shift from synthetic to real images, we trained different models using 6 different domain adaptation methods: DAN [Long et al., 2015], JAN [Long et al., 2017], CDAN [Long et al., 2018], MDD [Zhang et al., 2019], SAFN [Xu et al., 2019], MCC [Jin et al., 2020]. The results are shown in Table 4. We find that our STS method provides the best calibration error, followed by our SAC method.

8.4 Ablation study on SAC

Our SAC method is based on two key components: using corrupted data for calibration, and adaptive calibration based on the model’s mean confidence. In order to measure the contribution of each component we can compare SAC to the STS and TS. The results show that STS improves upon TS at higher levels of corruption intensity, thus proving the effectiveness of surrogate calibration sets. However, this comes at the cost of poorer calibration at low corruption intensities. The SAC method

Table 3: ECE % (lower is better) comparison on target data not seen during training on *Office-Home* with different domain adaptation methods.

	A2C	A2P	A2R	C2A	C2P	C2R	P2A	P2C	P2R	R2A	R2C	R2P	Avg
Vanilla	27.88	17.42	6.70	13.26	13.07	10.81	12.75	26.07	5.45	7.49	20.90	5.62	13.95
TS	28.08	17.88	8.39	11.09	10.97	8.72	15.07	27.06	6.10	6.32	21.37	5.63	13.89
CPCS	18.18	17.33	9.36	10.22	10.21	15.88	10.18	34.26	11.38	7.42	17.12	5.12	13.89
TransCal	10.76	16.26	14.65	12.50	11.32	6.38	9.56	22.34	5.80	7.09	9.51	8.85	11.25
SAC (Ours)	28.08	17.88	8.39	11.14	10.89	8.14	17.72	29.44	7.41	6.56	20.54	5.63	14.32
STS (Ours)	25.23	15.26	4.86	10.2	11.47	7.90	14.55	27.97	5.28	6.03	15.95	4.94	12.47

Table 4: ECE % (lower is better) on target data not seen during training on *VisDA-2017* with different domain adaptation methods.

	DAN	JAN	CDAN	MDD	SAFN	MCC
Vanilla	21.10	27.46	18.44	23.34	22.93	23.58
TS	19.24	29.85	21.03	24.56	19.55	24.03
CPCS	6.67	31.04	21.89	24.17	25.78	24.53
TransCal	25.61	34.48	22.81	25.88	29.73	24.84
SAC (Ours)	7.83	23.66	18.68	22.72	7.05	23.32
STS (Ours)	5.33	20.03	9.04	18.11	9.45	22.38

not only provides bigger improvements in calibration at higher corruption intensities, it also retains calibration at lower intensities. This highlights the importance of the adaptive mechanism.

Why it works: Our results are based on the fact that we can use the model outputs, in our case simply the p^{\max} values, as a proxy to evaluate distribution shift. This was illustrated in Figure 1: the calibration set whose p^{\max} mean is closest to the p^{\max} mean of the test set typically has lower calibration error. This is precisely what our SAC method does.

9 Conclusions

Increasingly, models trained on a given dataset are being asked to perform on data from a “shifted” dataset. Our work focuses on calibration of uncertainty estimates: we wish to ensure the model’s output probability reflects the true probability of the event. In contrast to most deep uncertainty work, we use a (frustratingly easy) purely statistical approach, and successfully reduce the calibration error of deep image classifiers under dataset shift.

We propose 2 methods, where we add a simple extra calibration step, and estimate uncertainty using only the model outputs. Our calibration methods involve synthesizing surrogate calibration sets by simply adding increasing intensities of a single type of known corruption to the original calibration data. While one method leverages unlabeled target images to choose the best surrogate set, the other simply uses their union. Our methods only require the output probabilities of a model, unlike previous methods which typically require the features of a model. Moreover, our methods do not require any retraining or retuning or additional training.

While previous works have shown that uncertainty estimates degrade on corrupted data, our two proposed calibration methods lead to better calibration on various types of dataset shifts: synthetic, natural, and domain adaptation. This is evidenced quantitatively in extensive experiments.

References

- Shai Ben-David, John Blitzer, Koby Crammer, and Fernando Pereira. Analysis of representations for domain adaptation. In B. Schölkopf, J. Platt, and T. Hoffman, editors, *Advances in Neural Information Processing Systems*, volume 19. MIT Press, 2007. URL <https://proceedings.neurips.cc/paper/2006/file/b1b0432ceafb0ce714426e9114852ac7-Paper.pdf>.
- Shai Ben-David, John Blitzer, Koby Crammer, Alex Kulesza, Fernando Pereira, and Jennifer Wortman Vaughan. A theory of learning from different domains. *Machine Learning*, 79(1):151–175, 2010. doi: 10.1007/s10994-009-5152-4. URL <https://doi.org/10.1007/s10994-009-5152-4>.

- Charles Blundell, Julien Cornebise, Koray Kavukcuoglu, and Daan Wierstra. Weight uncertainty in neural network. In Francis Bach and David Blei, editors, *Proceedings of the 32nd International Conference on Machine Learning*, volume 37 of *Proceedings of Machine Learning Research*, pages 1613–1622, Lille, France, 07–09 Jul 2015. PMLR. URL <http://proceedings.mlr.press/v37/blunde1115.html>.
- Sanghyuk Chun, Seong Joon Oh, Sangdoon Yun, Dongyoon Han, Junsuk Choe, and Youngjoon Yoo. An empirical evaluation on robustness and uncertainty of regularization methods. *arXiv preprint arXiv:2003.03879*, 2020.
- Morris H DeGroot and Stephen E Fienberg. The comparison and evaluation of forecasters. *Journal of the Royal Statistical Society: Series D (The Statistician)*, 32(1-2):12–22, 1983.
- Pedro Domingos and Michael Pazzani. Beyond independence: Conditions for the optimality of the simple bayesian classifier. In *Proc. 13th Intl. Conf. Machine Learning*, pages 105–112, 1996.
- Yarin Gal and Zoubin Ghahramani. Dropout as a bayesian approximation: Representing model uncertainty in deep learning. In Maria Florina Balcan and Kilian Q. Weinberger, editors, *Proceedings of The 33rd International Conference on Machine Learning*, volume 48 of *Proceedings of Machine Learning Research*, pages 1050–1059, New York, New York, USA, 20–22 Jun 2016. PMLR. URL <http://proceedings.mlr.press/v48/gal16.html>.
- Yaroslav Ganin, Evgeniya Ustinova, Hana Ajakan, Pascal Germain, Hugo Larochelle, François Laviolette, Mario March, and Victor Lempitsky. Domain-adversarial training of neural networks. *Journal of Machine Learning Research*, 17(59):1–35, 2016. URL <http://jmlr.org/papers/v17/15-239.html>.
- Robert Geirhos, Carlos RM Temme, Jonas Rauber, Heiko H Schütt, Matthias Bethge, and Felix A Wichmann. Generalisation in humans and deep neural networks. In *Advances in neural information processing systems*, pages 7538–7550, 2018.
- Ian Goodfellow, Jean Pouget-Abadie, Mehdi Mirza, Bing Xu, David Warde-Farley, Sherjil Ozair, Aaron Courville, and Yoshua Bengio. Generative adversarial nets. In Z. Ghahramani, M. Welling, C. Cortes, N. Lawrence, and K. Q. Weinberger, editors, *Advances in Neural Information Processing Systems*, volume 27. Curran Associates, Inc., 2014. URL <https://proceedings.neurips.cc/paper/2014/file/5ca3e9b122f61f8f06494c97b1afccf3-Paper.pdf>.
- Alex Graves. Practical variational inference for neural networks. In J. Shawe-Taylor, R. S. Zemel, P. L. Bartlett, F. Pereira, and K. Q. Weinberger, editors, *Advances in Neural Information Processing Systems 24*, pages 2348–2356. Curran Associates, Inc., 2011.
- Arthur Gretton, Dino Sejdinovic, Heiko Strathmann, Sivaraman Balakrishnan, Massimiliano Pontil, Kenji Fukumizu, and Bharath K. Sriperumbudur. Optimal kernel choice for large-scale two-sample tests. In F. Pereira, C. J. C. Burges, L. Bottou, and K. Q. Weinberger, editors, *Advances in Neural Information Processing Systems*, volume 25. Curran Associates, Inc., 2012. URL <https://proceedings.neurips.cc/paper/2012/file/dbe272bab69f8e13f14b405e038deb64-Paper.pdf>.
- Chuan Guo, Geoff Pleiss, Yu Sun, and Kilian Q. Weinberger. On Calibration of Modern Neural Networks. In *Proceedings of the 34th International Conference on Machine Learning, ICML 2017, Sydney, NSW, Australia, 6-11 August 2017*, pages 1321–1330, 2017.
- Chirag Gupta, Aleksandr Podkopaev, and Aaditya Ramdas. Distribution-free binary classification: prediction sets, confidence intervals and calibration. In H. Larochelle, M. Ranzato, R. Hadsell, M. F. Balcan, and H. Lin, editors, *Advances in Neural Information Processing Systems*, volume 33, pages 3711–3723. Curran Associates, Inc., 2020. URL <https://proceedings.neurips.cc/paper/2020/file/26d88423fc6da243ffddf161ca712757-Paper.pdf>.
- Dan Hendrycks and Thomas Dietterich. Benchmarking neural network robustness to common corruptions and perturbations. *Proceedings of the International Conference on Learning Representations*, 2019.

- Dan Hendrycks and Kevin Gimpel. A baseline for detecting misclassified and out-of-distribution examples in neural networks. In *Proceedings of International Conference on Learning Representations*, 2017.
- Dan Hendrycks, Kimin Lee, and Mantas Mazeika. Using pre-training can improve model robustness and uncertainty. *Proceedings of the International Conference on Machine Learning*, 2019a.
- Dan Hendrycks, Mantas Mazeika, and Thomas Dietterich. Deep anomaly detection with outlier exposure. *Proceedings of the International Conference on Learning Representations*, 2019b.
- Dan Hendrycks, Norman Mu, Ekin D. Cubuk, Barret Zoph, Justin Gilmer, and Balaji Lakshminarayanan. AugMix: A simple data processing method to improve robustness and uncertainty. *Proceedings of the International Conference on Learning Representations (ICLR)*, 2020.
- Junguang Jiang, Baixu Chen, Bo Fu, and Mingsheng Long. Transfer-learning-library. <https://github.com/thuml/Transfer-Learning-Library>, 2020.
- Ying Jin, Ximei Wang, Mingsheng Long, and Jianmin Wang. Minimum class confusion for versatile domain adaptation. In Andrea Vedaldi, Horst Bischof, Thomas Brox, and Jan-Michael Frahm, editors, *Computer Vision – ECCV 2020*, pages 464–480, Cham, 2020. Springer International Publishing.
- Ranganath Krishnan and Omesh Tickoo. Improving model calibration with accuracy versus uncertainty optimization. In H. Larochelle, M. Ranzato, R. Hadsell, M. F. Balcan, and H. Lin, editors, *Advances in Neural Information Processing Systems*, volume 33, pages 18237–18248. Curran Associates, Inc., 2020. URL <https://proceedings.neurips.cc/paper/2020/file/d3d9446802a44259755d38e6d163e820-Paper.pdf>.
- Meelis Kull, Miquel Perello Nieto, Markus Kängsepp, Telmo Silva Filho, Hao Song, and Peter Flach. Beyond temperature scaling: Obtaining well-calibrated multi-class probabilities with dirichlet calibration. In H. Wallach, H. Larochelle, A. Beygelzimer, F. d'Alché-Buc, E. Fox, and R. Garnett, editors, *Advances in Neural Information Processing Systems*, volume 32. Curran Associates, Inc., 2019.
- Balaji Lakshminarayanan, Alexander Pritzel, and Charles Blundell. Simple and Scalable Predictive Uncertainty Estimation using Deep Ensembles. In *Advances in Neural Information Processing Systems 30: Annual Conference on Neural Information Processing Systems 2017, 4-9 December 2017, Long Beach, CA, USA*, pages 6405–6416, 2017.
- Tsung-Yi Lin, Michael Maire, Serge Belongie, James Hays, Pietro Perona, Deva Ramanan, Piotr Dollár, and C. Lawrence Zitnick. Microsoft coco: Common objects in context. In David Fleet, Tomas Pajdla, Bernt Schiele, and Tinne Tuytelaars, editors, *Computer Vision – ECCV 2014*, pages 740–755, Cham, 2014. Springer International Publishing.
- Mingsheng Long, Yue Cao, Jianmin Wang, and Michael I. Jordan. Learning transferable features with deep adaptation networks. In *Proceedings of the 32nd International Conference on International Conference on Machine Learning - Volume 37, ICML'15*, pages 97–105. JMLR.org, 2015.
- Mingsheng Long, Han Zhu, Jianmin Wang, and Michael I. Jordan. Deep transfer learning with joint adaptation networks. In Doina Precup and Yee Whye Teh, editors, *Proceedings of the 34th International Conference on Machine Learning*, volume 70 of *Proceedings of Machine Learning Research*, pages 2208–2217. PMLR, 06–11 Aug 2017. URL <http://proceedings.mlr.press/v70/long17a.html>.
- Mingsheng Long, ZHANGJIE CAO, Jianmin Wang, and Michael I Jordan. Conditional adversarial domain adaptation. In S. Bengio, H. Wallach, H. Larochelle, K. Grauman, N. Cesa-Bianchi, and R. Garnett, editors, *Advances in Neural Information Processing Systems*, volume 31. Curran Associates, Inc., 2018. URL <https://proceedings.neurips.cc/paper/2018/file/ab88b15733f543179858600245108dd8-Paper.pdf>.
- Christos Louizos and Max Welling. Structured and efficient variational deep learning with matrix gaussian posteriors. In Maria Florina Balcan and Kilian Q. Weinberger, editors, *Proceedings of The 33rd International Conference on Machine Learning*, volume 48 of *Proceedings of Machine*

- Learning Research*, pages 1708–1716, New York, New York, USA, 20–22 Jun 2016. PMLR. URL <http://proceedings.mlr.press/v48/louizos16.html>.
- Christos Louizos and Max Welling. Multiplicative normalizing flows for variational Bayesian neural networks. In Doina Precup and Yee Whye Teh, editors, *Proceedings of the 34th International Conference on Machine Learning*, volume 70 of *Proceedings of Machine Learning Research*, pages 2218–2227, International Convention Centre, Sydney, Australia, 06–11 Aug 2017. PMLR. URL <http://proceedings.mlr.press/v70/louizos17a.html>.
- Zachary Nado, Shreyas Padhy, D Sculley, Alexander D’Amour, Balaji Lakshminarayanan, and Jasper Snoek. Evaluating prediction-time batch normalization for robustness under covariate shift. In *ICML 2020 Workshop on Uncertainty and Robustness in Deep Learning*, 2020.
- Anh Mai Nguyen, Jason Yosinski, and Jeff Clune. Deep neural networks are easily fooled: High confidence predictions for unrecognizable images. In *IEEE Conference on Computer Vision and Pattern Recognition, CVPR 2015, Boston, MA, USA, June 7-12, 2015*, pages 427–436, 2015. doi: 10.1109/CVPR.2015.7298640. URL <https://doi.org/10.1109/CVPR.2015.7298640>.
- Jeremy Nixon, Michael W. Dusenberry, Linchuan Zhang, Ghassen Jerfel, and Dustin Tran. Measuring calibration in deep learning. In *Proceedings of the IEEE/CVF Conference on Computer Vision and Pattern Recognition (CVPR) Workshops*, June 2019.
- Yaniv Ovadia, Emily Fertig, Jie Ren, Zachary Nado, D. Sculley, Sebastian Nowozin, Joshua Dillon, Balaji Lakshminarayanan, and Jasper Snoek. Can you trust your model’s uncertainty? Evaluating predictive uncertainty under dataset shift. In H. Wallach, H. Larochelle, A. Beygelzimer, F. d’Alché Buc, E. Fox, and R. Garnett, editors, *Advances in Neural Information Processing Systems 32*, pages 13991–14002. Curran Associates, Inc., 2019.
- Sangdon Park, Osbert Bastani, James Weimer, and Insup Lee. Calibrated prediction with covariate shift via unsupervised domain adaptation. In Silvia Chiappa and Roberto Calandra, editors, *The 23rd International Conference on Artificial Intelligence and Statistics, AISTATS 2020, 26-28 August 2020, Online [Palermo, Sicily, Italy]*, volume 108 of *Proceedings of Machine Learning Research*, pages 3219–3229. PMLR, 2020. URL <http://proceedings.mlr.press/v108/park20b.html>.
- Xingchao Peng, Ben Usman, Neela Kaushik, Judy Hoffman, Dequan Wang, and Kate Saenko. Visda: The visual domain adaptation challenge. *CoRR*, *abs/1710.06924*, 2017.
- Amir Rahimi, Amirreza Shaban, Ching-An Cheng, Richard Hartley, and Byron Boots. Intra order-preserving functions for calibration of multi-class neural networks. In H. Larochelle, M. Ranzato, R. Hadsell, M. F. Balcan, and H. Lin, editors, *Advances in Neural Information Processing Systems*, volume 33, pages 13456–13467. Curran Associates, Inc., 2020.
- Benjamin Recht, Rebecca Roelofs, Ludwig Schmidt, and Vaishal Shankar. Do ImageNet classifiers generalize to ImageNet? In Kamalika Chaudhuri and Ruslan Salakhutdinov, editors, *Proceedings of the 36th International Conference on Machine Learning*, volume 97 of *Proceedings of Machine Learning Research*, pages 5389–5400. PMLR, 09–15 Jun 2019. URL <https://proceedings.mlr.press/v97/recht19a.html>.
- Oleg Sémary. Face recognition using pytorch. <https://github.com/osmr/imgclsmb>, 2021.
- Zhihui Shao, Jianyi Yang, and Shaolei Ren. Calibrating deep neural network classifiers on out-of-distribution datasets, 2020.
- Hidetoshi Shimodaira. Improving predictive inference under covariate shift by weighting the log-likelihood function. *Journal of Statistical Planning and Inference*, 90(2):227–244, 2000. ISSN 0378-3758. doi: [https://doi.org/10.1016/S0378-3758\(00\)00115-4](https://doi.org/10.1016/S0378-3758(00)00115-4). URL <https://www.sciencedirect.com/science/article/pii/S0378375800001154>.
- Nitish Srivastava, Geoffrey Hinton, Alex Krizhevsky, Ilya Sutskever, and Ruslan Salakhutdinov. Dropout: A simple way to prevent neural networks from overfitting. *Journal of Machine Learning Research*, 15:1929–1958, 06 2014.

- Igor Vasiljevic, Ayan Chakrabarti, and Gregory Shakhnarovich. Examining the impact of blur on recognition by convolutional networks. *arXiv preprint arXiv:1611.05760*, 2016.
- Hemanth Venkateswara, Jose Eusebio, Shayok Chakraborty, and Sethuraman Panchanathan. Deep hashing network for unsupervised domain adaptation. In *Proceedings of the IEEE Conference on Computer Vision and Pattern Recognition (CVPR)*, July 2017.
- Haohan Wang, Songwei Ge, Zachary Lipton, and Eric P Xing. Learning robust global representations by penalizing local predictive power. In *Advances in Neural Information Processing Systems*, pages 10506–10518, 2019.
- Ximei Wang, Mingsheng Long, Jianmin Wang, and Michael I. Jordan. Transferable calibration with lower bias and variance in domain adaptation. In *Advances in neural information processing systems*, 2020.
- Yeming Wen, Paul Vicol, Jimmy Ba, Dustin Tran, and Roger Grosse. Flipout: Efficient pseudo-independent weight perturbations on mini-batches. In *International Conference on Learning Representations*, 2018.
- Ruijia Xu, Guanbin Li, Jihan Yang, and Liang Lin. Larger norm more transferable: An adaptive feature norm approach for unsupervised domain adaptation. In *The IEEE International Conference on Computer Vision (ICCV)*, October 2019.
- Yuchen Zhang, Tianle Liu, Mingsheng Long, and Michael Jordan. Bridging theory and algorithm for domain adaptation. In Kamalika Chaudhuri and Ruslan Salakhutdinov, editors, *Proceedings of the 36th International Conference on Machine Learning*, volume 97 of *Proceedings of Machine Learning Research*, pages 7404–7413. PMLR, 09–15 Jun 2019. URL <http://proceedings.mlr.press/v97/zhang19i.html>.

Supplemental Material

A CIFAR-10-C and ImageNet-C

CIFAR-10-C and ImageNet-C [Hendrycks and Dietterich, 2019] are datasets obtained from the CIFAR-10 and ImageNet datasets, respectively, by applying common real-world corruptions at different levels of intensity. The corruptions considered in this work are: *Brightness*, *Contrast*, *Defocus Blur*, *Elastic Transform*, *Fog*, *Frost*, *Gaussian Blur*, *Gaussian Noise*, *Glass Blur*, *Impulse Noise*, *Pixelate*, *Saturate*, *Shot Noise*, *Spatter*, *Speckle Noise*, *Zoom Blur*. In Figure 3 we show an example of all the different corruptions. In Figure 4 we show the contrast corruption type in five different intensities.

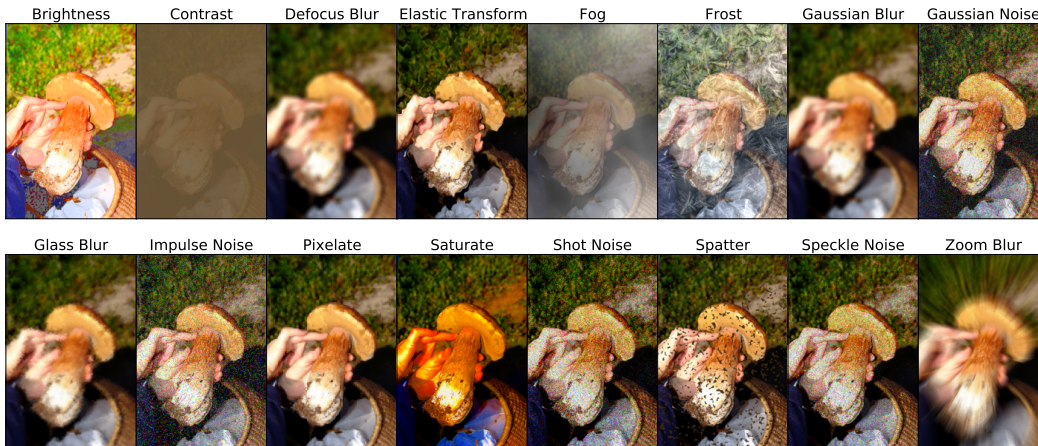


Figure 3: Example of the different 16 corruptions used to form CIFAR-10-C and ImageNet-C [Hendrycks and Dietterich, 2019].



Figure 4: Example of the contrast corruption at the different levels of intensity.

B Robustness to the choice of corruption

We look how the choice of corruption to synthesize the surrogate calibration sets impacts our methods. Ideally, the choice of corruption should be representative of the distribution of corruptions, so a mild corruption or a very strong corruption would give slightly worse results. At the same time, here we demonstrate that choosing a different corruption should not significantly degrade the results.

In Figure 5 we perform a cross-validation study over the choice of corruption used to generate the calibration sets (always leaving it out of the corruptions used at test time). We plot the mean and variance of the ECE across different validation corruptions types. We find that for CIFAR-10, our AAC method is robust to the choice of corruption. For the ImageNet model, the robust remains although a careful choice may be necessary at higher levels of corruption.

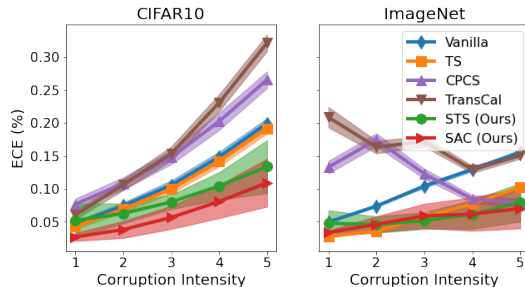


Figure 5: Mean ECE (lower is better), averaged across different corruption types used in making the calibration sets. Figure 2 shows us the mean ECE using “contrast” as the calibration corruption. Here we show how those means change when different corruptions are used in the calibration set. For CIFAR-10, our proposed methods are robust to the choice of corruption used in the calibration set, while for ImageNet the choice of the corruption is more important, in particular for the Single Image method.

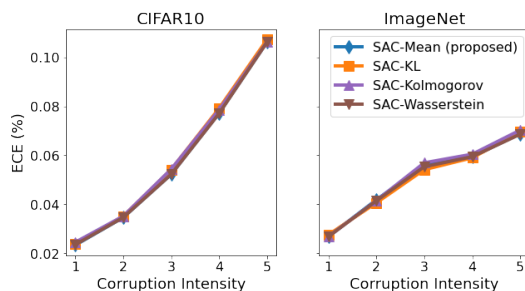


Figure 6: Comparison of different distances to choose the surrogate calibration set: Mean Expected Calibration Error (ECE) (lower is better) of the benchmark implementation [Ovadia et al., 2019], versus our Multi-Image methods for ImageNet (top) and CIFAR-10 (bottom). Each box represents a different uncertainty method.

C Variants of the SAC method

As discussed in subsection 7.3, the SAC method is robust to the choice of distributional distance to choose the surrogate calibration set (see Figure 6) and when using the mean only 100 samples are enough instead of the entire calibration set (see Figure 7).

D Qualitative Results

Figure 8 shows the calibrated probabilities for a typical test set. Figure 9 expands on Figure 2 by making use of a box-whisker plot to summarize the ECE across the different corruptions through its median and 1st and 3rd quantiles.

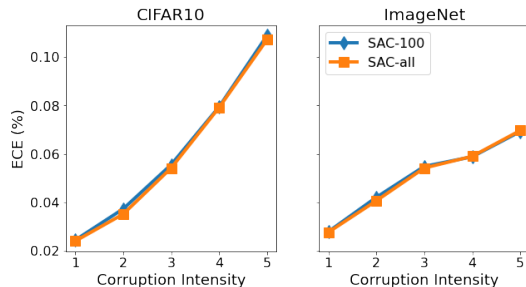


Figure 7: Comparison of our Multi-Image method for ImageNet (top) and CIFAR-10 (bottom) using the full batch of test images and only 100 of them, which we refer to as peak. Mean Expected Calibration Error (ECE) across different corruptions types, for fixed corruption intensity going from 0 to 5. Each box represents a different uncertainty method.

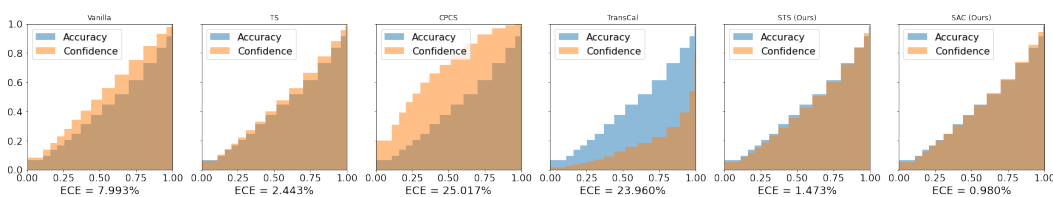


Figure 8: Calibration errors for the different methods on corrupted images on ImageNet using the elastic transform corruption with intensity 2. The x-axis is the range of p^{\max} values. We visualize as binned histograms the model accuracy (blue) (Equation 10), and the confidence estimates (orange) (Equation 11) (brown is where they overlap). The gap between the orange and blue curves represents the calibration error.

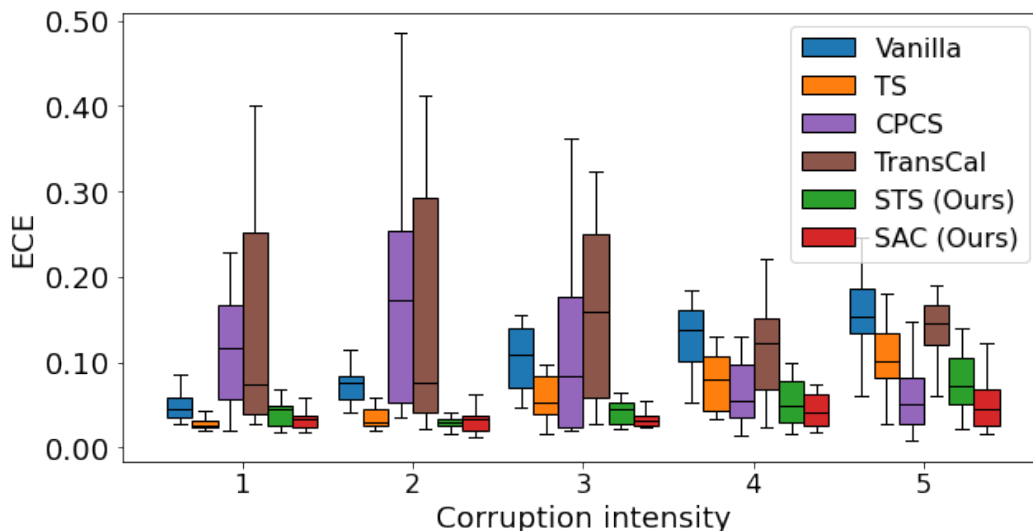


Figure 9: Comparison of the ECE (lower is better) for across corruptions types for 5 corruption intensities using different calibration methods: Vanilla, Temperature Scaling (TS), CPCS [Park et al., 2020], TransCal [Wang et al., 2020], our Surrogate Temperature Scaling (STS), and our Surrogate-Adaptive Calibration (SAC). Our methods perform the best among all methods across all intensities, with the greatest improvement at higher intensities. For each method, we show the quartiles summarizing the results on each corruption intensity. The ECE using our approaches is consistently better.